www.acsnano.org

# Site-Selective Deposition of Silica Nanoframes and Nanocages onto Faceted Gold Nanostructures Using a Primer-free Tetraethyl Orthosilicate Synthesis

Brendan D. Nieukirk, Runze Tang, Robert A. Hughes, and Svetlana Neretina\*



Downloaded via UNIV OF NOTRE DAME on July 10, 2024 at 13:38:15 (UTC). See https://pubs.acs.org/sharingguidelines for options on how to legitimately share published articles.

Cite This: https://doi.org/10.1021/acsnano.4c05258



**ACCESS** I

Metrics & More

Article Recommendations

Supporting Information

ABSTRACT: The Stöber method for forming spherical silica colloids is well-established as one of the pillars of colloidal synthesis. In a modified form, it has been extensively used to deposit both porous and protective shells over metal nanomaterials. Current best-practice techniques require that the vitreophobic surface of metal nanoparticles be primed with a surface ligand to promote silica deposition. Although such techniques have proved highly successful in forming core—shell configurations, the site-selective deposition of silica onto preselected areas of faceted metal nanostructures has proved far more challenging. Herein, a primer-free TEOS-based synthesis is demonstrated that is capable of forming architecturally complex nanoframes and nanocages on the pristine surfaces of faceted gold nanostructures. The devised synthesis overcomes vitreophobicity using elevated TEOS concen-













trations that trigger silica nucleation along the low-coordination sites where gold facets meet. Continued deposition sees the emergence of a well-connected frame followed by the lateral infilling of the openings formed over gold facets. With growth readily terminated at any point in this sequence, the synthesis distinguishes itself in being able to achieve patterned and tunable silica depositions expressing interfaces that are uncorrupted by primers. The so-formed structures are demonstrated as template materials capable of asserting high-level control over synthesis and assembly processes by using the deposited silica as a mask that deactivates selected areas against these processes while allowing them to proceed elsewhere. The work, hence, extends the capabilities and versatility of TEOS-based syntheses and provides pathways for forming multicomponent nanostructures and nanoassemblies with structurally engineered properties.

KEYWORDS: Stöber method, TEOS, nanoframe, nanocage, core-satellite, regioselective

ulticomponent nanostructures composed of metal and oxide segments express chemical, optical, and electrical properties that radically differ from those of their constituent materials. 1-9 Synergistic or collective behaviors can arise from the formation of (i) mesoporous or impermeable chemical layers, (ii) diffusion barriers, (iii) Schottky barriers, (iv) interfacial strain, (v) new or obstructed electron transfer pathways, and (vi) optically coupled responses. Derived from these emergent properties are a host of enabling capabilities that allow nanomaterials to operate in harsh chemical and thermal environments, attain biocompatibility, achieve colloidal stability and dispersibility, and realize enhanced light-harvesting capabilities. With a combined oxide-metal materials set that is both vast and complemented by a well-established group of mutually reliant and independent synthetic pathways, these multicomponent

systems have become an indispensable class of nanomaterials with applications in catalysis, <sup>3–6</sup> sensing, <sup>10–12</sup> biomedicine, <sup>2,13</sup> plasmonics, <sup>14,15</sup> environmental remediation, <sup>4,8</sup> and photovoltaic energy production, storage, and chemical conversion. <sup>8</sup>

The Stöber method<sup>16,17</sup> for synthesizing monodisperse silica nanoparticles utilizing a sol-gel process is a foundational approach for forming oxides in liquid media. The use of this method as a means to form silica shells over citrate-capped Au

Received: April 21, 2024 Revised: July 2, 2024 Accepted: July 5, 2024



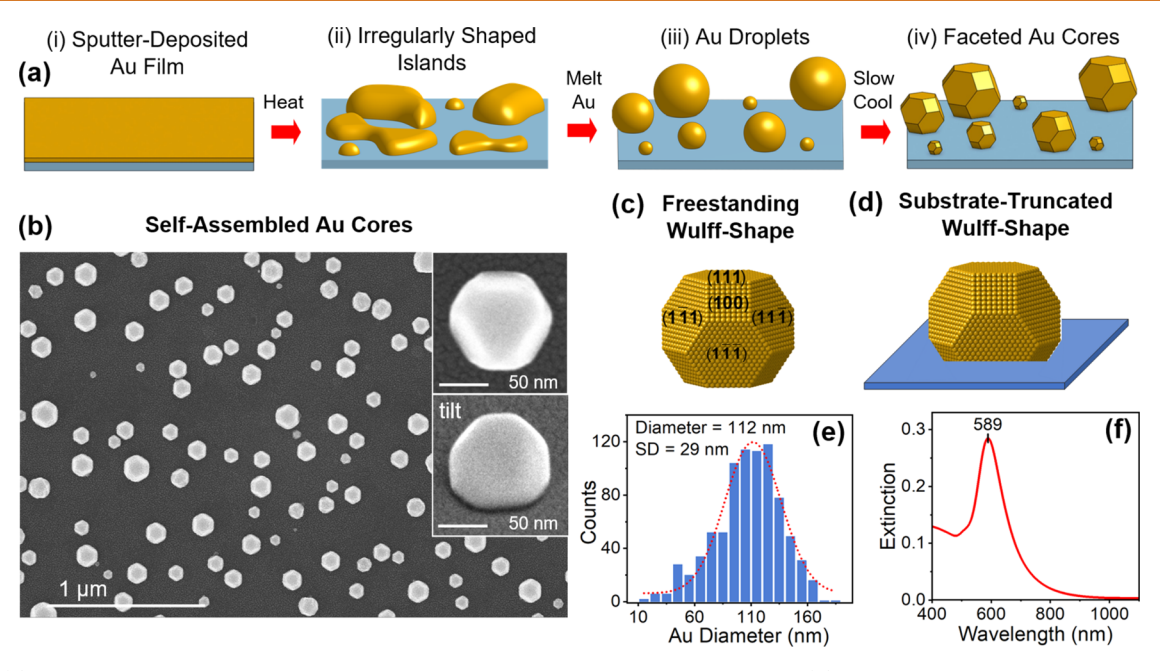


Figure 1. (a) Schematic of the self-assembly process used to form substrate-bound Au cores. (b) SEM images of the assembled cores where the insets show an individual structure from top and tilted views. Schematics showing a Wulff-shaped nanostructure that is (c) freestanding and (d) substrate-truncated where facets are identified. (e) Histogram of the Au core size distribution (SD is standard deviation). (f) Extinction spectrum for the assembled structures that shows a prominent plasmon resonance at 589 nm.

nanoparticles, however, faced significant hurdles because the vitreophobic nature of the Au surface favors the formation of core-free silica particles over the desired core—shell configuration and the tendency for citrate-capped Au nanoparticles to aggregate when transferred from aqueous to organic solvents. Liz-Marzán et al. 18 addressed these challenges by carrying out a citrate-to-aminosilane ligand exchange prior to silica deposition. The substitution offered colloidal stability while simultaneously priming the Au surface for silica growth. The devised scheme, commonly referred to as a modified Stöber process, now encompasses many variations to the approach 7,19 and proved instrumental in laying the foundation for the entire field dedicated to the formation of inorganic oxide shells on metal nanoparticles.

Current best practices for the modified Stöber process see presynthesized Au nanoparticles primed unless the nanoparticle stabilizing agent can provide this functionality (e.g., CTAB). Although numerous primers have been demonstrated,<sup>2</sup> polyvinylpyrrolidone (PVP) is widely accepted as a general-purpose primer because it has proven effective for a wide range of nanomaterials.<sup>20</sup> From the standpoint of the current investigation, it is noteworthy that there now exist several reports where thick silica shells have been formed on citrate-terminated Au nanoparticles despite the fact that citrate is considered ineffective as a primer. <sup>21–26</sup> Notwithstanding, a typical synthesis proceeds through the addition of primed Au nanoparticles to a mixture of tetraethyl orthosilicate (TEOS), ammonia, water, and an alcohol (e.g., ethanol, methanol, isopropanol). The ensuing reaction sees the ammoniacatalyzed hydrolysis of TEOS generate silica sols that condense upon the nanoparticle surface. A sufficient number of Au nanoparticles must exist within the growth solution to provide enough nucleation sites to suppress the formation of unwanted core-free silica nanoparticles. Also of significance is that the primer remains incorporated in the final core-shell product. The overall methodology has been applied to a broad range of metal nanostructures of varying size, shape, and composition.  $^{2,7}$ 

Although considerable progress has been made in the use of the modified Stöber method as a means to form concentric shells around metal nanostructures, the site-selective growth of silica onto preselected areas<sup>27</sup> has proved far more challenging. The importance of tailoring the deposition, such that portions of both the metal and oxide surfaces remain exposed, is that these configurations allow for the (i) synthesis of complex nanostructures using hard mask techniques whereby a secondary metal is deposited onto the exposed metal surface and (ii) selective etching of the metal component. Such strategies have allowed for the synthesis of symmetry-breaking nanomaterials, 28,29 bimorphic nanostructures, 30 Au nanocages,<sup>31</sup> and standalone oxide shells.<sup>32,33</sup> Additionally, Meyer et al.<sup>34</sup> have recently demonstrated that anisotropic silica coatings can give rise to enhanced SERS signals by concentrating analytes at the tips of Au nanorods. Currently, few examples exist where the TEOS-based syntheses have been used to selectively deposit silica onto metal nanostructures. 30,34-41 The strategies that have been put forth rely upon (i) competing ligands, 30,39 (ii) the dissimilar capping occurring between high- and low-curvature metal surfaces, 34-37,40 and (iii) the segregation of copolymers on nanometals.<sup>41</sup> For each case, silica deposition is preferred on one of the two contrasting areas of the functionalized nanometal surface. The silica formations derived from these methods are, however, somewhat unsophisticated in that they either form hemispherical coatings on spherical nanoparticles or roundish structures that protrude from the surface of faceted nanometals.

The modified Stöber process, while well-established in colloidal synthesis, has rarely been practiced on substrate-immobilized nanometals.<sup>42</sup> Much of this can be attributed to atomic layer deposition (ALD)<sup>43</sup> being highly amenable to the wafer-based processing of nanomaterials<sup>44</sup> while providing

similar and often superior capabilities in terms of generating conformal oxide layers over materials that are able to resist corrosion and oxidation, 45-47 withstand harsh thermal environments, 47,48 and allow for electrically insulating 44 or Schottky barriers. 49 ALD, however, also proves challenging from the standpoint of obtaining site-selective oxide formations, requiring either highly specialized techniques 50,51 or postsynthesis alterations such as directional ion milling.<sup>52</sup> Herein, a TEOS-based synthesis is presented that is capable of a highly controlled site-selective deposition over well-defined regions of faceted Au nanostructures in the absence of a primer layer. The so-formed structures are demonstrated in synthetic and assembly processes that utilize the oxide as a means to chemically deactivate selected areas while allowing these processes to proceed on the exposed Au surfaces. The work, hence, extends the versatility of the Stöber methodology and expands the techniques required to form structurally engineered nanomaterials.

# **RESULTS**

Solid-state dewetting 53,54 was utilized as a straightforward method for generating the substrate-bound cores needed for silica depositions. The process, which is shown schematically in Figure 1a, sees an ultrathin Au film sputter-deposited onto a [0001]-oriented sapphire substrate followed by a heating regimen that sees it rapidly heated to temperatures in excess of its melting point and then slow-cooled to room temperature over a 3 h period. The overall process sees the Au film break up into irregularly shaped nanoscale islands that, upon melting, realize droplet shapes that then go on to adopt well-formed facets during the cooldown period. The so-formed structures are well-bonded to the substrate and, as a result, are able to withstand sonication. Figure 1b shows an SEM image of the self-assembled Au cores where the insets display top and tilted views of a single structure. The observed faceting is consistent with the equilibrium shape expected for a substrate-bound face-centered cubic (fcc) single-crystal nanostructure<sup>55</sup> in that it appears as a Wulff shape expressing eight {111} and six {100} facets (Figure 1c) but where this shape is truncated where it intersects the surface of the substrate (Figure 1d). The structures show a strong tendency toward aligning on the substrate with their [111]-axis normal to the surface due to a heteroepitaxial relationship formed between (111) Au and (0001) sapphire.<sup>56</sup> It is, however, noted that heteroepitaxy is imperfect in that misaligned structures having their [100]- and [110]-axis normal to the substrate surface also appear in small quantities (vide infra). The assembly process gives rise to a Gaussian-like size distribution centered at a diameter of 112 nm with measured values ranging from 10 to 160 nm (Figure 1e). Spectroscopic characterization reveals a prominent localized surface plasmon resonance (LSPR) centered at 589 nm (Figure 1f).

When the core component is immobilized on the surface of a substrate, it becomes possible to carry out syntheses that profoundly differ from those used to form silica shells on Au colloids. A key difference is that the Au cores have pristine surfaces because they have never been exposed to a chemical environment other than air and Ar and, as such, can enter the reaction without stabilizing agents or be functionalized as desired. This difference allows cores to enter the reaction under conditions that, if applied to colloids, would lead to severe and irreversible aggregation. Maintaining core stability is, therefore, paramount for colloid-based synthesis whereas for

substrate-supported structures it is a nonfactor. In colloidal syntheses, cores are added at the concentrations needed to consume silica precursor species at a rate that forms core-shell structures while suppressing the unwanted formation of coreless structures.<sup>57</sup> There must, hence, be a delicate balance between reactant concentrations and core densities within the growth solution. In contrast, the formation of coreless silica structures is inevitable at any workable reactant concentrations for substrate-based syntheses because the number of cores on a reasonably sized substrate is orders of magnitude smaller than that typically used in colloidal synthesis. This seeming disadvantage is, however, made inconsequential by virtue of the fact that the populations of core-shell and coreless structures are easily separated by merely removing the substrate from the growth solution. This ease of separation turns out to be advantageous in that it allows for substratebased syntheses to be carried out under conditions that are problematic for colloid core-shell formation and, as such, broadens the permissible parameter space under which syntheses can be performed. The process by which the reaction is terminated is also fundamentally different in that substrate removal from the growth solution followed by a rapid rinse causes a near-instantaneous end to silica deposition whereas colloidal syntheses are terminated either by allowing the reaction to run to completion or through chemical quenching procedures<sup>21</sup> that make further deposition unlikely.

A modified Stöber method was used to deposit silica onto substrate-bound Au cores where reaction conditions were chosen to operate outside of the parameter windows typically used in the synthesis of colloidal Au@silica core-shell structures. Of specific importance is that the cores enter the reaction without the application of a primer and that TEOS concentrations greatly exceed those typically used in other primer-free syntheses (Table S1).<sup>21–26</sup> A standard synthesis proceeds by first placing one or more substrates supporting Au cores at the bottom of the 30 mL beaker containing ethanol (18.75 mL). Room-temperature silica growth is then initiated through the sequential addition of H<sub>2</sub>O (2.39 mL), ammonium hydroxide (28% NH<sub>3</sub>, 0.25 mL), and TEOS (0.34 mL) under constant stirring. For any given sample, the reaction is terminated through its removal from the growth solution whereupon it is rinsed in ethanol and air-dried. It should be noted that reactants are oversupplied to such an extent that the simultaneous growth of multiple samples does not create any sort of competition for reactants since less than 0.005% of the Si within the growth solution is deposited onto a single sample. The use of multiple samples, which are removed from the growth solution at set intervals, is advantageous in that it allows for a time series that is representative of a growth progression in a manner that is analogous to the aliquot extraction procedure commonly used in colloidal syntheses.

Numerous syntheses were carried out where multiple substrates were placed in the silica growth solution and then sequentially removed to obtain an understanding of the growth mode. SEM imaging was then used to examine the as-grown structures as well as identical structures that were exposed to an aqua regia etch that selectively removes the Au component. The etching procedure, whose viability is demonstrated over large areas in Figure S1, was adopted in this study because the remaining standalone silica structures more clearly highlight the site-selective nature of the silica deposition. The earliest stages of silica deposition onto the Au cores results in a discontinuous patchwork of islands (Figure S2) that lack

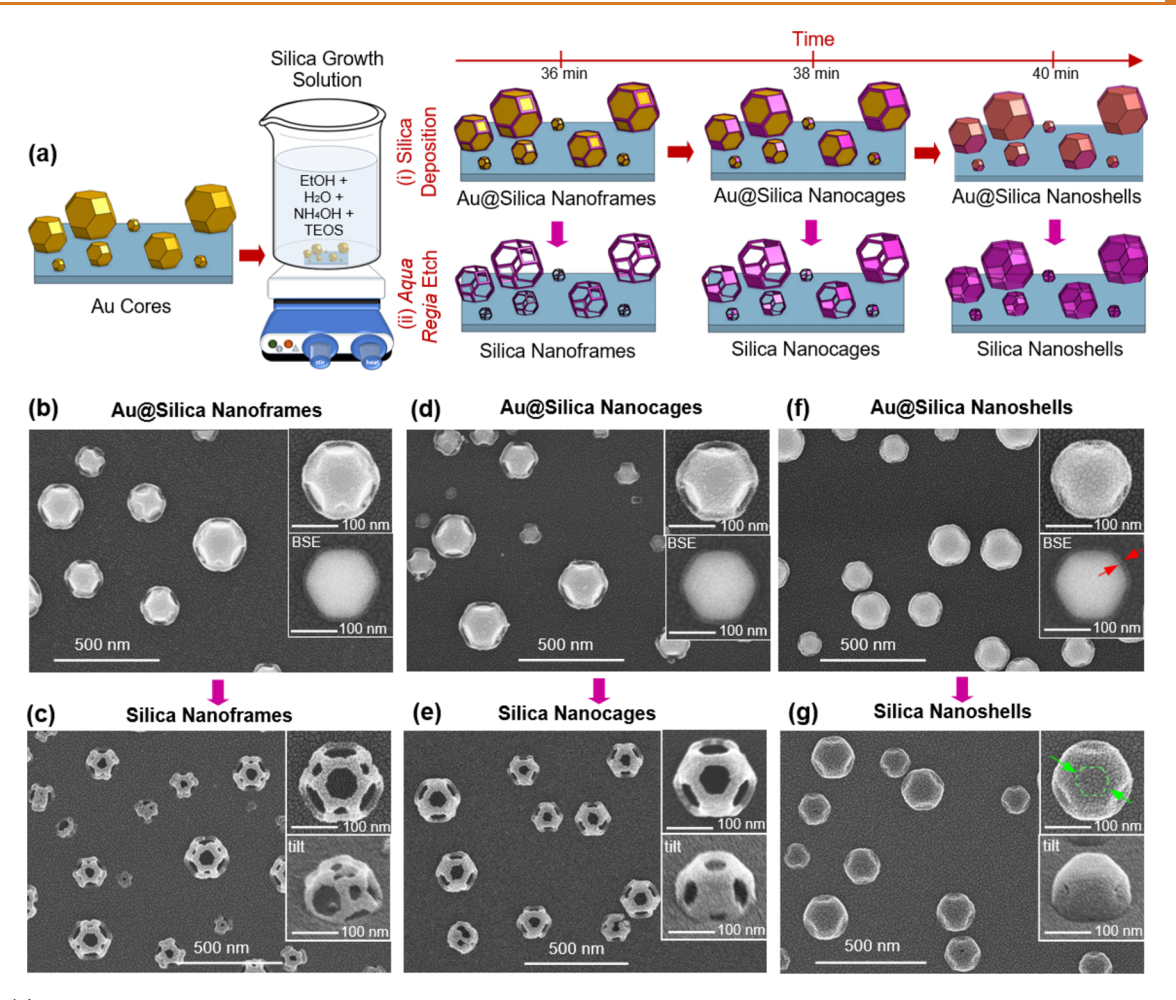


Figure 2. (a) Schematics showing the time evolution of silica deposition onto Wulff-shaped Au cores occurring for synthesis times of 36, 38, and 40 min as well as the standalone silica structures obtained when the Au component is removed with *aqua regia*. SEM images of the Au@ silica and standalone silica structures expressing the (b,c) nanoframe, (d,e) nanocage, and (f,g) nanoshell geometry. The insets to Figure 2b,d,f show top-view SEM images of individual structures along with BSE images whereas those of Figure 2c,e,g show individual structures from top and tilted views.

structural integrity when the etching procedure is carried out. As deposition continues, there is, however, a 4 min time interval between 36 and 40 min where the depositing shells become continuous while rapidly undergoing morphological transformations. Figure 2 provides both SEM images and schematic illustrations of the structures formed for silica depositions that are terminated at critical time points occurring at the beginning, middle, and end of this period. Observed are three distinct shell morphologies that are referred to as nanoframes, nanocages, and nanoshells. It should be noted that these critical time points are repeatable in duration from synthesis-to-synthesis provided that the size distribution and spacing of the Au nanostructures remains constant. Alterations to these parameters can significantly shift optimal timing requirements (Figure S3). Additionally, there exists a size dependence whereby smaller diameter structures follow the same growth pathway but where the {100} and {111} openings fill in at a faster rate, a result that is not surprising given that the openings are smaller in size and, hence, require less deposition to become sealed.

The site-selective nature of the silica deposition is most apparent for the nanoframe geometry in that it closely follows the topography defined by the ridge pattern where the various facets of the Wulff-shaped Au core intersect (Figure 2b). At

this stage, there exist two distinct sets of openings where the larger corresponds to the locations that {111} Au facets occupy while the smaller corresponds to the {100} facets. The nanoframe morphology becomes more easily discernible when the Au component is etched away, leaving behind standalone silica structures that remain bonded to the substrate surface (Figure 2c). The transformation from a nanoframe to a nanocage structure occurs as a result of the {100} facet openings filling in laterally from their perimeter such that the remaining silica structures only have openings at the Au {111} facet locations (Figure 2d,e). It is noteworthy that a comparison of the backscattered electron (BSE) SEM images for individual structures (Figure 2b,d, insets) indicates that the nanoframe-to-nanocage transformation occurs without any significant thickening of the silica layer. Further deposition sees the {111} openings close to form a continuous conformal shell but where the silica deposited on these facets is significantly thinner (Figure 2f). The BSE SEM images, once again, indicate that the overgrowth of these openings is achieved without significant shell thickening (Figure 2f, inset). The nanoshells, while encapsulating the entire core, remain sufficiently porous to facilitate the complete removal of the Au core with an etchant, albeit at significantly longer etching times (Figure 2g). An examination of the spectroscopic response for each of these

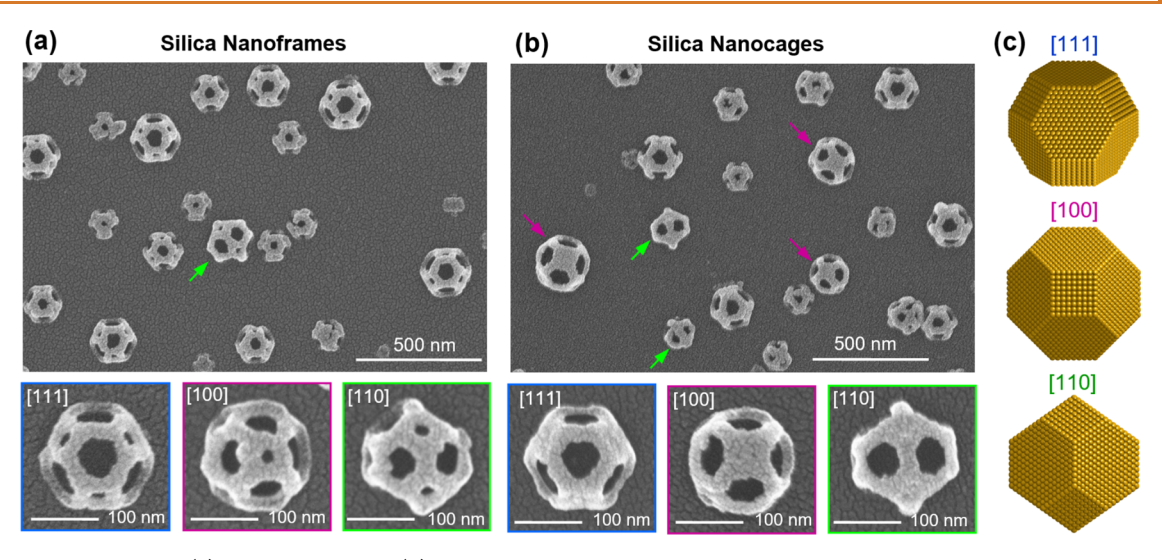


Figure 3. Standalone silica (a) nanoframes and (b) nanocages showing distinctive architectures depending upon the crystallographic orientation of the Au core relative to the surface of the substrate. (c) Schematics showing top-down perspectives of the same Wulff-shaped Au core when its [111]-, [100]-, and [110]-axis is perpendicular to the surface of the substrate. It should be noted that the openings in the silica nanoframes and nanocages closely follow the displayed facet pattern.

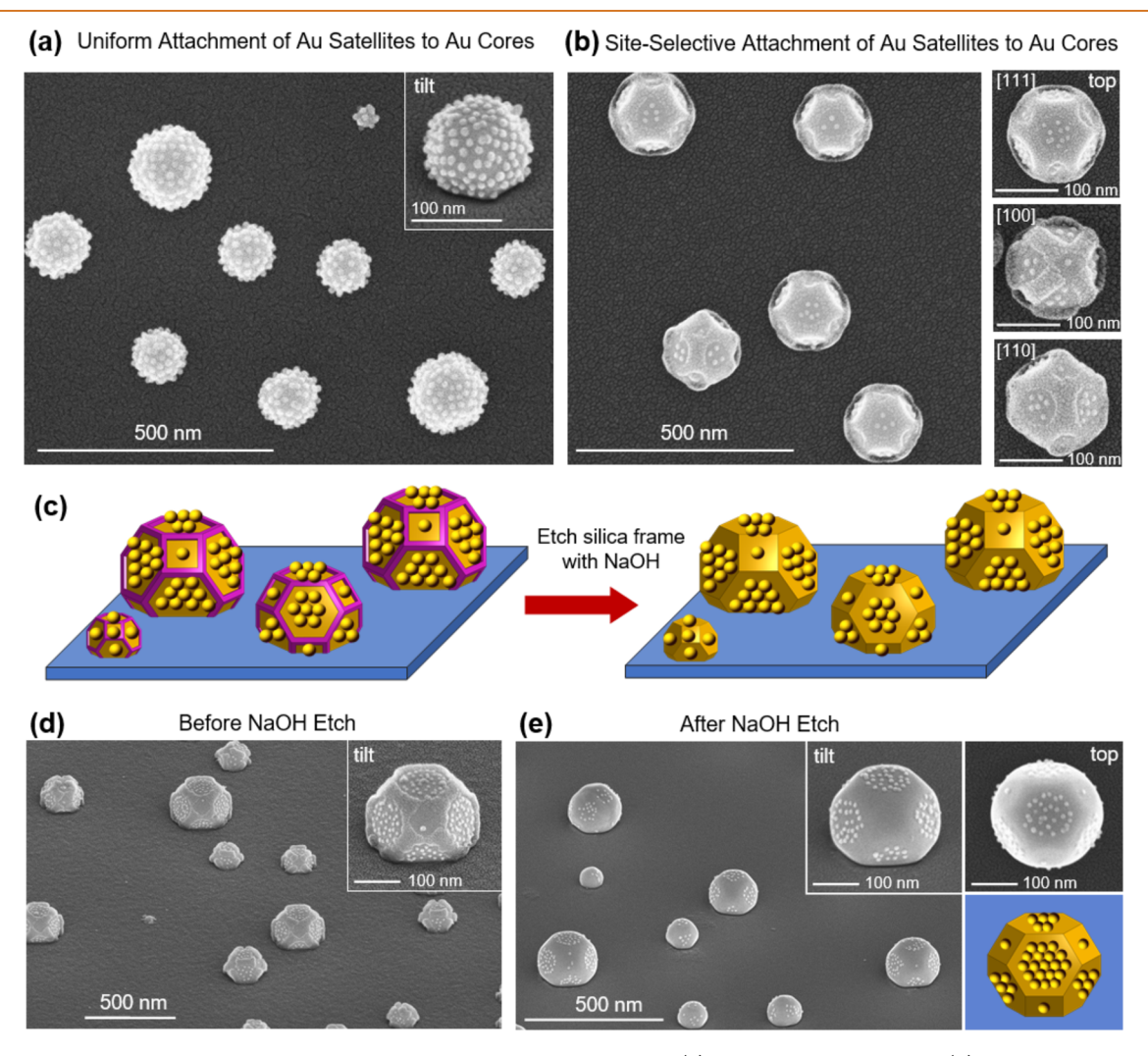


Figure 4. SEM images of Au core-satellite structures that were assembled using (a) as-formed Au cores and (b) identical cores onto which silica nanoframes are deposited. (c) Schematic illustration of the silica nanoframe removal process using a NaOH etch. Tilted-view SEM images of the core-satellite configurations (d) before and (e) after silica removal.

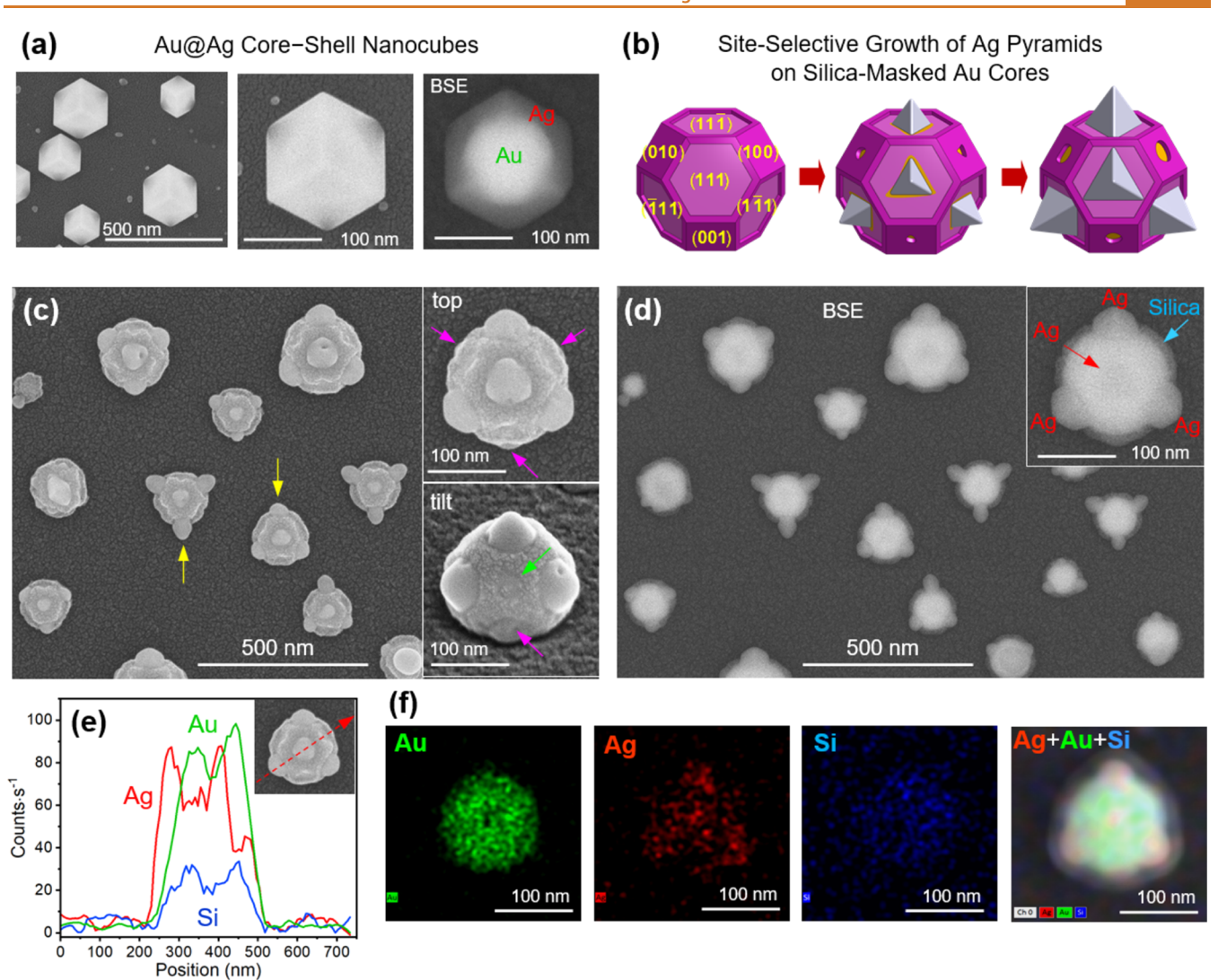


Figure 5. (a) SEM and BSE images of Au@Ag core—shell nanocubes. (b) Schematic showing the morphological progression occurring when a Wulff-shaped Au core is coated with a nonuniform silica shell and then immersed in a growth solution that causes silica hydrolysis followed by Ag deposition. (c) SEM and (d) BSE images of the nanostructures formed. EDS analysis performed on a single structure in the form of elemental (e) line scans and (f) maps.

three structures indicates that the plasmon shifts are all similarly valued at approximately 20 nm (Figure S4), a result that is consistent with a lack of shell thickening as the topology transforms from nanoframe to nanoshell. It should be noted that these syntheses are accompanied by a silica deposition onto the sapphire substrate and the formation of silica colloids with mean diameters of 36 nm (Figure S5).

Syntheses were carried out where the concentrations of TEOS,  $H_2O$ , and  $NH_3$  were varied. It was determined that the use of high TEOS concentrations is the critical requirement for the site-selective growth of silica onto pristine Au surfaces, without which silica growth is patchy and irregular even for syntheses lasting 24 h (Figure S6). At this point, the reactants are highly depleted since an additional 24 h sees little increase in the diameter of the spherical silica colloids within the growth solution ( $d_{24h} = 79 \pm 7$  nm,  $d_{48h} = 82 \pm 6$  nm). At high TEOS concentrations, the high reaction barrier for the adsorption of silica precursors onto the vitreophobic surface of Au is overcome but only at sites of high curvature where there exists an abundance of low-coordination sites caused by the rounding that occurs where dissimilar facets meet on dewetted

Au structures.<sup>58</sup> Once silica islands are formed, lateral growth proceeds in a manner that follows the surface energy landscape of the Au core in that high surface energy ridges are coated first, followed by the infilling of the openings on the {100} and {111} facets. The anisotropy in the silica growth is highlighted by the fact that the silica shell remains quite thin (Figure 2f, red arrows) when compared to the extent of the lateral growth that is needed to, for example, overgrow the {111} facets (Figure 2g, green arrows). Lateral silica growth along the Au facets is, hence, preferred over silica-on-silica growth that is normal to the Au surface. Variations to the H<sub>2</sub>O and NH<sub>3</sub> concentrations reveal fairly wide parameter windows where the growth mode remains intact (Figure S7).

The Au@silica nanoframes and nanocages formed through this site-selective deposition of silica onto Wulff-shaped Au cores stand out as being the most architecturally complex structures ever grown using a modified Stöber process and, as such, have no colloidal analog. They also distinguish themselves in that the Au—silica interface is uncorrupted by primers or stabilizing agents. Moreover, the removal of the Au core through a selective etch leaves behind amorphous silica

structures that express some of the same geometric symmetries as fcc crystals. This point is exemplified by the set of silica nanoframes and nanocages shown in Figure 3a,b. These images show standalone silica structures that take on different geometric forms depending on whether the initial Au core is oriented with its [111]-, [100]- or [110]-axis perpendicular to the surface of the substrate as shown in the schematics in Figure 3c. All the structures shown, hence, follow the same growth pattern in that the openings on the nanoframes are at the locations occupied by the {111} and {100} facets of the Au core whereas the openings on nanocages appear at just {111} facet positions. This collection of structures, from a purely morphological standpoint, emulate the nanometal architectures derived from the galvanic replacement of substrate-based single-crystal Ag nanostructures with Au and share commonalities with a host of metal nanoframe and nanocage architectures realized through various colloidal chemistries.  $^{59-61}$ 

The site-selective deposition of silica onto Wulff-shaped Au nanostructures offers the opportunity to deterministically position nanoscale objects on just the exposed Au surfaces. As an initial demonstration, a core-satellite assembly process was carried out in both the presence and absence of silica nanoframes. The core-satellite motif consists of a central core structure onto which many smaller satellite nanoparticles are tethered using molecular linkers. This configuration allows for the formation of numerous plasmonic nanogaps with nanometer-scale widths on a single structure and, as such, has become one of the most often synthesized and applied multicomponent nanoassemblies. 62-64 The core-satellite assembly process sees dewetted Au structures (i.e., the cores) functionalized with 1,8-octanedithiol (C8DT) linkers and then immersed into a Turkevich-synthesized<sup>65</sup> colloid of Au nanoparticles that, once attached, serve as satellites. This assembly process, in its unadulterated form, realizes substratebound Au cores that are densely populated with satellites (Figure 4a). It is important to note that the sapphire substrate remains free of satellite particles because the C8DT linker is unable to bind to the oxide surface. When the same assembly process is carried out using Au cores onto which silica nanoframes are deposited, the C8DT linker functionalizes the exposed Au surfaces while showing no affinity for the silicacoated areas. As a result, satellite attachment occurs only on the unprotected Au surfaces while being obstructed elsewhere (Figure 4b). After assembly, core structures having their [111]-, [100]- and [110]-axis normal to the substrate surface each exhibit a distinctive core-satellite morphology (Figure 4b, insets). The amorphous nature of the deposited silica makes it susceptible to etching in aqueous NaOH. This allows for the postassembly process shown schematically in Figure 4c in which the silica nanocage is completely removed, leaving behind Au cores that exhibit both bare and satellite-laden areas. Figure 4d,e shows top-down and tilted-view SEM images of core-satellite structures that are intricately decorated with satellite particles using this methodology. The overall assembly process, when spectroscopically tracked, sees a red shift in the plasmon resonance resulting from the addition of silica nanoframes and Au satellites followed by a blue shift when the nanoshell is removed (Figure S8).

In a second proof of concept demonstration, Au@silica nanostructures were used in a synthesis that sees the oxide act as a barrier to growth while allowing metal deposition to proceed on exposed Au surfaces. The overall scheme shares

similarities with Janus structure syntheses that proceed through the site-selective growth of a silica mask onto one side of a metal nanostructure followed by the reduction of a second metal onto the unmasked areas. <sup>39,40,66</sup> The synthesis presented here, however, leads to a far more sophisticated product due to the topographical complexity of the deposited silica. For this demonstration, a synthesis was chosen that, in its unadulterated form, realizes Au@Ag core-shell structures with a cube-like morphology. The aqueous synthesis, which is described in detail elsewhere, 52,67 sees Ag<sup>+</sup> ions reduced by citrate onto substrate-bound Au nanostructures at 95 °C. The so-formed structures, which are displayed as SEM and BSE images in Figure 5a, exhibit crisp (100) faceting, a sharp Au-Ag interface, and a nanocube orientation that sees one corner of the cube point away from the substrate surface due to the [111]-orientation of the Au core relative to the underlying substrate.

When the same synthesis is carried out on Au cores onto which silica nanoframes are deposited, it is challenged by the fact that silica grown by the modified Stober method is prone to a hydrolysis process that results in a loss of material when exposed to H<sub>2</sub>O.<sup>68</sup> Thus, when silica nanoframes are exposed to the 95 °C aqueous Ag growth solution, the structures disintegrate over the course of the synthesis to the point that it no longer acted as an effective mask. To circumvent this issue, Au nanostructures were coated with silica nanoshells instead of nanoframes using deposition times of 1 h. When exposed to the Ag growth solution, silica is still lost to hydrolysis but, in this case, the {111} Au facets become exposed because the silica layer is thinner at these locations while the remaining framework is sufficiently thick to endure the entire duration of the synthesis (Figure 5b). The overall process, when spectroscopically tracked, sees a 30 nm red shift in the LSPR resulting from silica deposition, followed by a 31 nm blue shift due to the combined influences of Ag deposition and the partial loss of silica (Figure S9).

Figure 5c displays an SEM image of the reaction product obtained when the Au@Ag core-shell nanocube synthesis is practiced on silica-protected Au cores where the insets show high-resolution images of a single structure from top and tilted views. The product deviates from the core-shell morphology in that Ag deposition appears as weakly faceted pyramids at the sites where the {111} Au facets were exposed to the growth solution. Deposition elsewhere is inhibited either by the silica nanoframe or through the capping of any Ag deposited on the exposed {100} Au facets (denoted by green arrow). Despite a considerable variation in size, the structures shown in Figure 5c exhibit a high degree of uniformity in terms of shape. Also evident is their in-plane alignment relative to the underlying substrate, consistently appearing in one of two orientations offset by 180° (denoted by yellow arrows). This alignment originates from the two equivalent heteroepitaxial relationships formed between Au and the [0001]-oriented sapphire substrate.<sup>56</sup> Apart from the four prominent pyramids appearing in top-down images, there also exist three smaller Ag pyramids at the base of the structure (locations denoted by magenta arrows). The BSE image of the same structures, shown in Figure 5d, more clearly highlights the elemental distribution, as both the Ag pyramids and silica shell stand out against the high-Z Au core. The overall morphology is confirmed by elemental line scans and mapping derived from energydispersive spectroscopy (EDS) measurements (Figure 5e,f). The Ag line scan, which was chosen to follow the path denoted

by the red arrow in the inset of the figure, shows two prominent peaks corresponding to the side and top pyramids as well as a smaller peak that is associated with the pyramid at the base of the structure. The Au and Si scans, as anticipated, both show a dip near the center of the structure. The elemental maps show a well-defined Au core, Ag pyramids, and a rather weak Si signature that, when overlaid, reveal the overall configuration of the structure. It is, however, difficult to discern from this data whether the {100} facets are exposed. To demonstrate that this is indeed the case, a core-satellite assembly process identical to that described in Figure 4 was carried out. The resulting nanoassembly not only shows satellite attachment to both the Ag pyramids and exposed {100} facets (Figure S10) but also realizes a multicomponent system with added architectural complexity. Taken together, these results show the effectiveness of the silica mask in deterministically steering growth modes toward otherwise unrealizable end points through site-selective depositions.

# **DISCUSSION**

The current report describes a TEOS-based deposition of silica onto Au nanostructures that distinguishes itself in terms of the synthesis performed, the product obtained, and the growth mode observed. Using substrate-bound nanostructures instead of Au colloids, syntheses are carried out in a regime where (i) nanostructure aggregation is avoided, (ii) TEOS concentrations are maintained at unusually high levels, (iii) unwanted silica colloids form but prove inconsequential, and (iv) reactions are terminated in a near-instantaneous manner. Operating within this regime allows for silica to be deposited on Au in the absence of primers and, as such, provides a more mechanistically pure depiction of the interactions between TEOS-generated silica sols and Au nanostructures. Standout features of the silica deposition include a curvature-driven nucleation process that leads to the site-selective deposition of a framework that follows the contours formed by the intersection of Au facets and a subsequent Au encapsulation process that is characterized by the lateral infilling of openings. The fact that lateral infilling proceeds at a rate that exceeds silica-on-silica growth that is normal to the surface stands out in relation to a literature that consistently shows site-selective growth that is characterized by isotropic growth fronts from which roundish nodules emerge. <sup>21,30,34–41</sup> This lateral growth is somewhat surprising given that silica, because it is amorphous, has no inherent growth direction. The most likely explanation is that silica precursor adsorption is strongly favored at the locations where the high-curvature edges of the silica nanoframe meet the surface of the Au facets. Such a preference would allow for the radial infilling of openings that would see {100} facets fill in first because the openings are smaller to begin with. The subsequent overgrowth of the {111} facets then rids the surface of strongly curved features without significant nanoshell thickening. This overall tendency toward growth patterns that lower curvature is consistent with the observation that extended TEOS-based depositions realize spherical core-shell structures even when the Au core is as architecturally complex as a nanostar.<sup>69</sup>

With the site-selective deposition of silica nanoframes and nanocages onto faceted Au nanostructures yielding structures that present two chemically distinct surfaces, the resulting configuration is readily exploited in the formation of designer nanoparticles and assemblies that utilize silica as a masking material. The so-formed structures, when compared to those

demonstrated using previously demonstrated masking techniques, realize exposed metal surfaces that present specific facets and, hence, allow for asymmetric growth modes. Such growth modes have proved decisive in generating an entire class of nanomaterials with coveted properties. This work also provides the impetus for determining whether the observed growth mode is adaptable to other oxides and metals. Such capabilities would allow for the synthesis of hybrid nanostructures composed of select metal components that are framed by semiconductor oxides (e.g., TiO<sub>2</sub>, CeO<sub>2</sub>) and, in doing so, provide an alternate design space for a class of materials that are renowned for their light-harvesting and photocatalytic capabilities.

# **CONCLUSIONS**

In summary, we have demonstrated a primer-free TEOS-based synthesis that enables the deposition of architecturally complex silica formations on faceted Au nanostructures. By using substrate-bound nanostructures with pristine surfaces instead of ligand-capped Au colloids, syntheses are carried out in a regime where silica nucleation and growth are driven by the topography of the Au surface. As a consequence, silica depositions onto Wulff-shaped Au nanostructures give rise to distinctive nanoframe, nanocage, and nanoshell architectures. The ability of such structures to steer synthesis and assembly processes toward previously unrealizable, yet predictable, end points is demonstrated. Taken together, this work advances the solution-based techniques needed for the site-selective deposition of oxide materials and highlights their use in the rational design of multicomponent nanostructures and nanoassemblies.

# **METHODS**

Chemicals and Materials. [0001]-oriented sapphire substrates were sourced from MTI Corporation as double-side polished, 100 mm diameter wafers that were then diced into 10.5 mm  $\times$  10 mm  $\times$ 0.65 mm pieces. Au films were deposited from a 19 mm diameter target that was punched from a 1.0 mm thick foil with 99.9985% purity (Thermo Scientific). Au core assembly was carried out in ultrahigh purity Ar (Airgas). Chemical reagents used in syntheses and assembly processes include tetraethyl orthosilicate (TEOS, MilliporeSigma), ammonium hydroxide (28% NH<sub>3</sub>, Thermo Scientific), deionized water (DI H2O, VWR), ethanol (Denatured, HPLC grade, VWR), hydrogen tetrachloroaurate(III) trihydrate (HAuCla·3H2O, 99.99% trace metal basis, Beantown Chemical), trisodium citrate dihydrate (Na<sub>3</sub>C<sub>6</sub>H<sub>5</sub>O<sub>7</sub>·2H<sub>2</sub>O, 99% pure, Thermo Scientific), potassium chloride (KCl, Sigma-Aldrich), 1,8-octanedithiol (C8DT, Fisher Scientific), silver nitrate (AgNO<sub>3</sub>, reagent ACS, Ward's Science), hydrochloric acid (6 M HCl, VWR), nitric acid (2 M HNO<sub>3</sub>, Beantown Chemical), and sulfuric acid (H<sub>2</sub>SO<sub>4</sub>, 95-98% ACS Reagent, VWR).

**Au Core Assembly.** Immediately prior to use, sapphire substrates are pretreated with a 60 s  ${\rm H_2SO_4}$  etch, rinsed in DI  ${\rm H_2O}$ , and dried under an  ${\rm N_2}$  gas flow. Polycrystalline Au films are sputter-deposited onto the substrates to a layer thickness of 18 nm. As many as 6 substrates are placed in an alumina boat, inserted into a tube furnace, and heated to elevated temperatures under an Ar gas flow of 170 cm<sup>3</sup>·min<sup>-1</sup>. After a 2 h room-temperature Ar purge of residual air within the tube, Au core assembly proceeds by rapidly raising the temperature to 1085 °C (27 min) and then slow cooling the assembled structures using a 3 h linearly ramped cooldown. Samples are typically cleaved into smaller pieces such that multiple silica syntheses can be carried out on identically assembled cores.

Silica Nanoframe, Nanocage, and Nanoshell Synthesis. The optimized synthesis of silica onto Wulff-shaped Au cores begins with the addition of 18.75 mL of ethanol into a 30 mL Pyrex beaker

containing a 1.5 cm Teflon magnetic stir bar. Up to four substrates are then placed at the bottom of the beaker at locations that do not interfere with the motion of the stir bar. The room-temperature silica synthesis is then initiated through the sequential addition of H<sub>2</sub>O (2.39 mL), ammonium hydroxide (28% NH<sub>3</sub>, 0.25 mL), and TEOS (0.34 mL) under continuous stirring (600 rpm). Silica deposition is terminated for each sample at preset time intervals (nanoframe: 36 min, nanocage: 38 min, nanoshell: 40 min) through its removal from the growth solution whereupon it is rinsed in ethanol before being airdried. For instances where standalone silica nanoframes, nanocages, and nanoshells were desired, Au core removal occurred through the placement of the sample in an aqua regia etch (Hazard: highly toxic and corrosive). Etch times of 5 min sufficed for nanoframes and nanocages whereas nanoshells required up to 20 min. Visible during Au core removal is a loss of sample color as the plasmonic response of the steadily shrinking cores is extinguished. Due to the fragility of the standalone shells, it is important that they be first submerged in DI H<sub>2</sub>O and then, while wet, be transferred to acetone. The displacement of H<sub>2</sub>O with acetone allows for a far gentler drying process since the capillary forces, which can cause damage, are significantly reduced.<sup>5</sup>

Core-Satellite Assembly. The Au nanoparticles that serve as satellite structures were prepared as a colloid using the Turkevich method.<sup>65</sup> The reaction proceeds through the rapid injection of trisodium citrate (12.5 mL, 34 mM) into a boiling mixture of HAuCl<sub>4</sub> (1.25 mL, 100 mM) and H<sub>2</sub>O (220 mL) that is continuously stirred at 350 rpm using a 5 cm PTFE-coated magnetic stir bar. After 10 min, the wine-red colloid is removed from the hot plate and allowed to naturally cool to room temperature under overnight stirring. Coresatellite assembly proceeded along a stepwise pathway that sees substrate-bound cores (i) immersed in an ethanolic solution of the C8DT linker (0.2 mM, 1.5 mL) for 30 min, (ii) sequentially rinsed in ethanol and water, (iii) immersed for 1 h in the Turkevichsynthesized Au colloid (2 mL) to which aqueous KCl (10 mM, 0.1 mL) was added, and (iv) removed from the colloid and rinsed in ethanol and dried under a N2 gas flow. Detailed procedures for both the Turkevich synthesis and core-satellite assembly process are described elsewhere.63

Site-Selective Ag Depositions. Au-silica core-shell structures were prepared using the aforementioned procedures except that the growth time was extended to 1 h to obtain silica structures that are able to withstand the hydrolysis that occurs throughout the synthesis. The synthesis proceeds in 10 mL Pyrex beakers by first preheating aqueous solutions of (i) AgNO<sub>3</sub> (1 mM, 3 mL), and (ii) trisodium citrate (10 mM, 1 mL) to which nitric acid (0.2 mM, 0.6 mL) is added. When the latter reaches the growth temperature of 95 °C, the substrate supporting the Au-silica core-shell structures is placed at the bottom of the beaker. After 30 s, the reaction is initiated through the addition of the AgNO<sub>3</sub> and allowed to proceed for 105 s. It is then terminated by removing the substrate from the growth solution, after which it is sonicated for a few seconds in room-temperature DI H<sub>2</sub>O to remove unwanted Ag colloid and dried under a N2 gas flow. Details regarding this synthesis as it relates to the formation of substratebased Au-Ag core-shell nanocubes are described elsewhere. 52,

**Instrumentation.** Au core assembly utilized a model 681 Gatan high resolution ion beam coater and a Lindberg Blue M furnace fitted with a quartz tube and an Ar gas handling system. A Helios G4 Ux SEM/FIB workstation (FEI) was used for SEM imaging and EDS analysis. Spectroscopic characterization utilized a JASCO V-730 UV—visible spectrophotometer.

# **ASSOCIATED CONTENT**

# Supporting Information

The Supporting Information is available free of charge at https://pubs.acs.org/doi/10.1021/acsnano.4c05258.

(a) SEM images showing the nanostructure morphologies obtained under a variety of synthesis conditions, (b) Extinction spectra of the nanostructures produced, (c) characterization of the silica colloids, (d) Table

comparing reactant concentrations for the primer-free syntheses of Au@silica core-shell nanostructures reported in the literature (PDF)

### **AUTHOR INFORMATION**

# **Corresponding Author**

Svetlana Neretina — Department of Chemistry and Biochemistry, University of Notre Dame, Notre Dame, Indiana 46556, United States; College of Engineering, University of Notre Dame, Notre Dame, Indiana 46556, United States; Occid.org/0000-0002-6889-4384; Email: sneretina@nd.edu

# **Authors**

Brendan D. Nieukirk — Department of Chemistry and Biochemistry, University of Notre Dame, Notre Dame, Indiana 46556, United States; orcid.org/0009-0009-8238-8726

Runze Tang – College of Engineering, University of Notre Dame, Notre Dame, Indiana 46556, United States

Robert A. Hughes — College of Engineering, University of Notre Dame, Notre Dame, Indiana 46556, United States

Complete contact information is available at: https://pubs.acs.org/10.1021/acsnano.4c05258

### **Notes**

The authors declare no competing financial interest.

# **ACKNOWLEDGMENTS**

This work was supported by the National Science Foundation, Division of Chemistry, Macromolecular, Supramolecular, and Nanochemistry (MSN) Program under Grant No. CHE-2107728 and the Division of Civil, Mechanical and Manufacturing Innovation (CMMI), Advanced Manufacturing (AM) Program, under Grant No. CMMI-2207664 to S.N. It has also benefited from the facilities available through the Notre Dame Integrated Imaging Facility (NDIIF).

# **REFERENCES**

- (1) Mendes, P. C. D.; Song, Y.; Ma, W.; Gani, T. Z. H.; Lim, K. H.; Kawi, S.; Kozlov, S. M. Opportunities in the Design of Metal@Oxide Core-Shell Nanoparticles. *Adv. Phys.* **2023**, *8*, No. 2175623.
- (2) Kim, M. J.; Jung, D. H.; Lee, C. Y.; Hong, S.; Heo, J. H.; Lee, J. H. Structurally Engineered Silica Shells on Gold Nanorods for Biomedical Applications. *Small Struct.* **2023**, *4*, No. 2300047.
- (3) Gao, C.; Lyu, F.; Yin, Y. Encapsulated Metal Nanoparticles for Catalysis. Chem. Rev. 2021, 121, 834–881.
- (4) Mondal, K.; Sharma, A. Recent Advances in the Synthesis and Application of Photocatalytic Metal—Metal Oxide Core—Shell Nanoparticles for Environmental Remediation and their Recycling Process. RSC Adv. 2016, 6, 83589—83612.
- (5) Lukosi, M.; Zhu, H.; Dai, S. Recent Advances in Gold-Metal Oxide Core-Shell Nanoparticles: Synthesis, Characterization, and their Application for Heterogeneous Catalysis. *Front. Chem. Sci. Eng.* **2016**, *10*, 39–56.
- (6) Li, G.; Tang, Z. Noble Metal Nanoparticle@Metal Oxide Core/Yolk— Shell Nanostructures as Catalysts: Recent Progress and Perspective. *Nanoscale* **2014**, *6*, 3995—4011.
- (7) Hanske, C.; Sanz-Ortiz, M. N.; Liz-Marzán, L. M. Silica-Coated Plasmonic Metal Nanoparticles in Action. *Adv. Mater.* **2018**, *30*, No. 1707003.
- (8) Liu, X.; Iocozzia, J.; Wang, Y.; Cui, X.; Chen, Y.; Zhao, S.; Li, Z.; Lin, Z. Noble Metal—Metal Oxide Nanohybrids with Tailored Nanostructures for Efficient Solar Energy Conversion, Photocatalysis

- and Environmental Remediation. Energy Environ. Sci. 2017, 10, 402–434.
- (9) Liu, S.; Regulacio, M. D.; Tee, S. Y.; Khin, Y. W.; Teng, C. P.; Koh, L. D.; Guan, G.; Han, M.-Y. Preparation, Functionality, and Application of Metal Oxide-coated Noble Metal Nanoparticle. *Chem. Rec.* **2016**, *16*, 1965–1990.
- (10) Li, J.-F.; Zhang, Y.-J.; Ding, S.-Y.; Panneerselvam, R.; Tian, Z. Q. Core-Shell Nanoparticle-Enhanced Raman Spectroscopy. *Chem. Rev.* **2017**, *117*, 5002–5069.
- (11) Zhang, H.; Duan, S.; Radjenovic, P. M.; Tian, Z.-Q.; Li, J.-F. Core—Shell Nanostructure-Enhanced Raman Spectroscopy for Surface Catalysis. *Acc. Chem. Res.* **2020**, *53*, 729–739.
- (12) Haryanto, A.; Lee, C. W. Shell Isolated Nanoparticle Enhanced Raman Spectroscopy for Mechanistic Investigation of Electrochemical Reactions. *Nano Convergence* **2022**, *9*, No. 9.
- (13) Liu, J.; Detrembleur, C.; De Pauw-Gillet, M.-C.; Mornet, S.; Jérôme, C.; Duguet, E. Gold Nanorods Coated with Mesoporous Silica Shell as Drug Delivery System for Remote Near Infrared Light-Activated Release and Potential Phototherapy. *Small* **2015**, *11*, 2323–2332.
- (14) Ha, M.; Kim, J.-H.; You, M.; Li, Q.; Fan, C.; Nam, J.-M. Multicomponent Plasmonic Nanoparticles: From Heterostructured Nanoparticles to Colloidal Composite Nanostructures. *Chem. Rev.* **2019**, *119*, 12208–12278.
- (15) Li, J.-F.; Li, C.-Y.; Aroca, R. F. Plasmon-Enhanced Fluorescence Spectroscopy. *Chem. Soc. Rev.* **2017**, *46*, 3962–3979.
- (16) Stöber, W.; Fink, A.; Bohn, E. Controlled Growth of Monodisperse Silica Spheres in the Micron Size Range. *J. Colloid Interface Sci.* **1968**, 26, 62–69.
- (17) Han, Y.; Lu, Z.; Teng, Z.; Liang, J.; Guo, Z.; Wang, D.; Han, M.-Y.; Yang, W. Unraveling the Growth Mechanism of Silica Particles in the Stöber Method: In Situ Seeded Growth Model. *Langmuir* **2017**, 33, 5879–5890.
- (18) Liz-Marzán, L. M.; Giersig, M.; Mulvaney, P. Synthesis of Nanosized Gold-Silica Core-Shell Particles. *Langmuir* **1996**, *12*, 4329–4335.
- (19) Liu, S.; Han, M. Y. Silica-Coated Metal Nanoparticles. *Chem. Asian J.* **2010**, *5*, 36–45.
- (20) Graf, C.; Vossen, D. L. J.; Imhof, A.; Van Blaaderen, A. A General Method to Coat Colloidal Particles with Silica. *Langmuir* **2003**, *19*, 6693–6700.
- (21) Engelbrekt, C.; Gargasya, Y.; Law, M. Silica Shell Growth on Vitreophobic Gold Nanoparticles Probed by Plasmon Resonance Dynamics. *J. Phys. Chem. C* **2021**, *125*, 25119–25125.
- (22) Kobayashi, Y.; Inose, H.; Nakagawa, T.; Gonda, K.; Takeda, M.; Ohuchi, N.; Kasuya, A. Synthesis of Au–Silica Core–Shell Particles by Sol–Gel Process. *Surf. Eng.* **2012**, *28*, 129–133.
- (23) Ye, J.; Van de Broek, B.; De Palma, R.; Libaers, W.; Clays, K.; Van Roy, W.; Borghs, G.; Maes, G. Surface Morphology Changes on Silica-Coated Gold Colloids. *Colloids Surf., A* **2008**, 322, 225–233.
- (24) Liu, S. H.; Han, M. Synthesis, Functionalization, and Bioconjugation of Monodisperse, Silica-Coated Gold Nanoparticles: Robust Bioprobes. *Adv. Funct. Mater.* **2005**, *15*, 961–967.
- (25) Lee, H. B.; Yoo, Y. M.; Han, Y.-H. Characteristic Optical Properties and Synthesis of Gold-Silica Core-Shell Colloids. *Scr. Mater.* **2006**, *55*, 1127–1129.
- (26) Lu, Y.; Yin, Y.; Li, Z.-Y.; Xia, Y. Synthesis and Self-Assembly of Au@SiO<sub>2</sub> Core-Shell Colloids. *Nano Lett.* **2002**, *2*, 785–788.
- (27) Hoang, K. N. L.; McClain, S. M.; Meyer, S. M.; Jalomo, C. A.; Forney, N. B.; Murphy, C. J. Site-Selective Modification of Metallic Nanoparticles. *Chem. Commun.* **2022**, *58*, 9728–9741.
- (28) Yang, X. Q.; Lu, Y.; Liu, Y.; Wang, J.; Shao, L.; Wang, J. F. Heterostructures Built through Site-Selective Deposition on Anisotropic Plasmonic Metal Nanocrystals and Their Applications. *Small Struct.* **2021**, *2*, No. 2100101.
- (29) Qiu, J.; Nguyen, Q. N.; Lyu, Z.; Wang, Q.; Xia, Y. Bimetallic Janus Nanocrystals: Syntheses and Applications. *Adv. Mater.* **2022**, *34*, No. 2102591.

- (30) Rodríguez-Fernández, D.; Altantzis, T.; Heidari, H.; Bals, S.; Liz-Marzán, L. M. A Protecting Group Approach Toward Synthesis of Au–Silica Janus Nanostars. *Chem. Commun.* **2014**, *50*, 79–81.
- (31) Hubert, C.; Chomette, C.; Désert, A.; Madeira, A.; Perro, A.; Florea, I.; Ihiawakrim, D.; Ersen, O.; Lombardi, A.; Pertreux, E.; Vialla, F.; Maioli, P.; Crut, A.; Del Fatti, N.; Vallée, F.; Majimel, J.; Ravaine, S.; Duguet, E.; Tréguer-Delapierre, M. Versatile Template-Directed Synthesis of Gold Nanocages with a Predefined Number of Windows. *Nanoscale Horiz.* **2021**, *6*, 311–318.
- (32) Gao, C.; Zhang, Q.; Lu, Z.; Yin, Y. Templated Synthesis of Metal Nanorods in Silica Nanotubes. J. Am. Chem. Soc. 2011, 133, 19706–19709.
- (33) Tuff, W. J.; Hughes, R. A.; Nieukirk, B. D.; Ciambriello, L.; Neal, R. D.; Golze, S. D.; Gavioli, L.; Neretina, S. Periodic Arrays of Structurally Complex Oxide Nanoshells and Their Use as Substrate-Confined Nanoreactors. *Nanoscale* **2023**, *15*, 17609–17620.
- (34) Meyer, S. M.; Murphy, C. J. Anisotropic Silica Coating on Gold Nanorods Boosts their Potential as SERS Sensors. *Nanoscale* **2022**, 14, 5214–5226.
- (35) Adelt, M.; MacLaren, D. A.; Birch, D. J. S.; Chen, Y. Morphological Changes of Silica Shells Deposited on Gold Nanorods: Implications for Nanoscale Photocatalysts. *ACS Appl. Nano Mater.* **2021**, *4*, 7730–7738.
- (36) Wang, M.; Hoff, A.; Doebler, J. E.; Emory, S. R.; Bao, Y. Dumbbell-Like Silica Coated Gold Nanorods and Their Plasmonic Properties. *Langmuir* **2019**, *35*, 16886–16892.
- (37) Huang, C.-M.; Chung, M.-F.; Souris, J. S.; Lo, L.-W. Controlled Epitaxial Growth of Mesoporous Silica/Gold Nanorod Nanolollipops and Nanodumb-Bells. *APL Mater.* **2014**, *2*, No. 113312.
- (38) Rowe, L. R.; Chapman, B. S.; Tracy, J. B. Understanding and Controlling the Morphology of Silica Shells on Gold Nanorods. *Chem. Mater.* **2018**, *30*, 6249–6258.
- (39) Chen, T.; Chen, G.; Xing, S.; Wu, T.; Chen, H. Scalable Routes to Janus Au-SiO<sub>2</sub> and Ternary Ag-Au-SiO<sub>2</sub> Nanoparticles. *Chem. Mater.* **2010**, 22, 3826–3828.
- (40) Wang, F.; Cheng, S.; Bao, Z.; Wang, J. Anisotropic Overgrowth of Metal Heterostructures Induced by a Site-Selective Silica Coating. *Angew. Chem.* **2013**, *125*, 10534–10538.
- (41) Zhang, Y.; Dong, W.; Wang, Y.; Wu, Q.; Yi, C.; Yang, Y.; Xu, Y.; Nie, Z. Synthesis of Patchy Nanoparticles with Symmetry Resembling Polar Small Molecules. *Small Methods* **2022**, *6*, No. 2200545.
- (42) Vinnacombe-Willson, G. A.; Conti, Y.; Stefancu, A.; Weiss, P. S.; Cortés, E.; Scarabelli, L. Direct Bottom-Up In Situ Growth: A Paradigm Shift for Studies in Wet-Chemical Synthesis of Gold Nanoparticles. *Chem. Rev.* **2023**, *123* (13), 8488–8529.
- (43) Johnson, R. W.; Hultqvist, A.; Bent, S. F. A Brief Review of Atomic Layer Deposition: From Fundamentals to Applications. *Mater. Today* **2014**, *17*, 236–246.
- (44) Prakash, J.; Swart, H. C.; Zhang, G.; Sun, S. Emerging Applications of Atomic Layer Deposition for the Rational Design of Novel Nanostructures for Surface-Enhanced Raman Scattering. *J. Mater. Chem. C* **2019**, *7*, 1447–1471.
- (45) Preston, A. S.; Hughes, R. A.; Demille, T. B.; Neretina, S. Plasmonics under Attack: Protecting Copper Nanostructures from Harsh Environments. *Chem. Mater.* **2020**, *32*, 6788–6799.
- (46) Daubert, J. S.; Hill, G. T.; Gotsch, H. N.; Gremaud, A. P.; Ovental, J. S.; Williams, P. S.; Oldham, C. J.; Parsons, G. N. Corrosion Protection of Copper Using Al<sub>2</sub>O<sub>3</sub>, TiO<sub>2</sub>, ZnO, HfO<sub>2</sub>, and ZrO<sub>2</sub> Atomic Layer Deposition. ACS Appl. Mater. Interfaces **2017**, *9*, 4192–4201.
- (47) Preston, A. S.; Hughes, R. A.; Dominique, N. L.; Camden, J. P.; Neretina, S. Stabilization of Plasmonic Silver Nanostructures with Ultrathin Oxide Coatings Formed Using Atomic Layer Deposition. *J. Phys. Chem. C* **2021**, *125*, 17212–17220.
- (48) Albrecht, G.; Ubl, M.; Kaiser, S.; Giessen, H.; Hentschel, M. Comprehensive Study of Plasmonic Materials in the Visible and Near-Infrared: Linear, Refractory, and Nonlinear Optical Properties. *ACS Photonics* **2018**, *5*, 1058–1067.

- (49) Zeng, X.; Zhao, Y.; Hu, X.; Stucky, G. D.; Moskovits, M. Rational Component and Structure Design of Noble-Metal Composites for Optical and Catalytic Applications. *Small Struct.* **2021**, *2*, No. 2000138.
- (50) Yasmeen, S.; Ryu, S.; Lee, S.-H.; Lee, H.-B.-R. Atomic Layer Deposition Beyond Thin Film Deposition Technology. *Adv. Mater. Technol.* **2022**, *9*, No. 2200876.
- (51) Mackus, A. J. M.; Merkx, M. J. M.; Kessels, W. M. M. From the Bottom-Up: Toward Area-Selective Atomic Layer Deposition with High Selectivity. *Chem. Mater.* **2019**, *31*, 2–12.
- (52) Tuff, W. J.; Hughes, R. A.; Golze, S. D.; Neretina, S. Ion Beam Milling as a Symmetry-Breaking Control in the Synthesis of Periodic Arrays of Identically Aligned Bimetallic Janus Nanocrystals. *ACS Nano* 2023, 17, 4050–4061.
- (53) Farzinpour, P.; Sundar, A.; Gilroy, K. D.; Eskin, Z. E.; Hughes, R. A.; Neretina, S. Altering the Dewetting Characteristics of Ultrathin Gold and Silver Films using a Sacrificial Antimony Layer. *Nanotechnology* **2012**, *23*, No. 495604.
- (54) Thompson, C. V. Solid-State Dewetting of Thin Films. Annu. Rev. Mater. Res. 2012, 42, 399-434.
- (55) Henry, C. R. Morphology of Supported Nanoparticles. *Prog. Surf. Sci.* **2005**, *80*, 92–116.
- (56) Golze, S. D.; Hughes, R. A.; Menumerov, E.; Rouvimov, S.; Neretina, S. Synergistic Roles of Vapor- and Liquid-Phase Epitaxy in the Seed-Mediated Synthesis of Substrate-Based Noble Metal Nanostructures. *Nanoscale* **2021**, *13*, 20225–20233.
- (57) Yoon, S.; Lee, B.; Kim, C.; Lee, J. H. Controlled Heterogeneous Nucleation for Synthesis of Uniform Mesoporous Silica-Coated Gold Nanorods with Tailorable Rotational Diffusion and 1 nm-Scale Size Tunability. *Cryst. Growth Des.* **2018**, *18*, 4731–4736.
- (58) Preston, A. S.; Hughes, R. A.; Demille, T. B.; Rey Davila, V. M.; Neretina, S. Dewetted Nanostructures of Gold, Silver, Copper, and Palladium with Enhanced Faceting. *Acta Mater.* **2019**, *165*, 15–25.
- (59) Gilroy, K. D.; Sundar, A.; Farzinpour, P.; Hughes, R. A.; Neretina, S. Mechanistic Study of Substrate-Based Galvanic Replacement Reactions. *Nano Res.* **2014**, *7*, 365–379.
- (60) Yang, T. H.; Ahn, J.; Shi, S.; Wang, P.; Gao, R.; Qin, D. Noble-Metal Nanoframes and Their Catalytic Applications. *Chem. Rev.* **2021**, 121. 796–833.
- (61) Skrabalak, S. E.; Chen, J.; Sun, Y.; Lu, X.; Au, L.; Cobley, C. M.; Xia, Y. Gold Nanocages: Synthesis, Properties, and Applications. *Acc. Chem. Res.* **2008**, *41*, 1587–1595.
- (62) Yoon, J. H.; Lim, J.; Yoon, S. Controlled Assembly and Plasmonic Properties of Asymmetric Core-Satellite Nanoassemblies. *ACS Nano* **2012**, *6*, 7199–7208.
- (63) Tang, R.; Hughes, R. A.; Tuff, W. J.; Corcoran, A.; Neretina, S. Rapid Formation of Gold Core—Satellite Nanostructures Using Turkevich-Synthesized Satellites and Dithiol Linkers: The Do's and Don'ts for Successful Assembly. *Nanoscale Adv.* **2024**, *6*, 3632–3643.
- (64) Gu, Q.; Zhu, J.; Weng, G.-J.; Li, J.-J.; Zhao, J.-W. Core-Satellite Nanostructures and their Biomedical Applications. *Microchim. Acta* **2022**, *189*, No. 470.
- (65) Wuithschick, M.; Birnbaum, A.; Witte, S.; Sztucki, M.; Vainio, U.; Pinna, N.; Rademann, K.; Emmerling, F.; Kraehnert, R.; Polte, J. Turkevich in New Robes: Key Questions Answered for the Most Common Gold Nanoparticle Synthesis. *ACS Nano* **2015**, *9*, 7052–7071.
- (66) Crane, C. C.; Tao, J.; Wang, F.; Zhu, Y.; Chen, J. Mask-Assisted Seeded Growth of Segmented Metallic Heteronanostructures. *J. Phys. Chem. C* 2014, *118*, 28134–28142.
- (67) Hajfathalian, M.; Gilroy, K. D.; Hughes, R. A.; Neretina, S. Citrate-Induced Nanocubes: A Reexamination of the Role of Citrate as a Shape-Directing Capping Agent for Ag-Based Nanostructures. *Small* **2016**, *12*, 3444–3452.
- (68) Hu, Y.; Zhang, Q.; Goebl, J.; Zhang, T.; Yin, Y. Control Over the Permeation of Silica Nanoshells by Surface-Protected Etching with Water. *Phys. Chem. Chem. Phys.* **2010**, *12*, 11836–11842.

- (69) Atta, S.; Rangan, S.; Fabris, L. Highly Tunable Growth and Etching of Silica Shells on Surfactant-Free Gold Nanostars. *ChemNanoMat* **2020**, *6*, 53–57.
- (70) Nguyen, Q. N.; Wang, C.; Shang, Y.; Janssen, A.; Xia, Y. Colloidal Synthesis of Metal Nanocrystals: From Asymmetrical Growth to Symmetry Breaking. *Chem. Rev.* **2023**, *123*, 3693–3760.
- (71) Kumar, A.; Choudhary, P.; Kumar, A.; Camargo, P. H. C.; Krishnan, V. Recent Advances in Plasmonic Photocatalysis Based on TiO<sub>2</sub> and Noble Metal Nanoparticles for Energy Conversion, Environmental Remediation, and Organic Synthesis. *Small* **2022**, *18*, No. 2101638.